

Electronic Spectra and Reversible Photoisomerization of Protonated Naphthalenes in Solid Neon

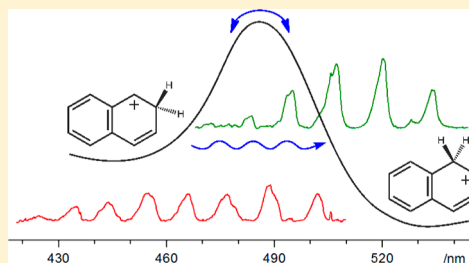
Iryna Garkusha,[†] Adam Nagy,[†] Jan Fulara,^{†,‡} Michal F. Rode,[‡] Andrzej L. Sobolewski,[‡] and John P. Maier^{*,†}

[†]Department of Chemistry, University of Basel, Klingelbergstrasse 80, CH-4056 Basel, Switzerland

[‡]Institute of Physics, Polish Academy of Sciences, Al. Lotników 32/46, PL-02668 Warsaw, Poland

S Supporting Information

ABSTRACT: Alpha- and beta-protonated naphthalenes (α - and β -HN⁺) were investigated by electronic absorption and fluorescence spectroscopies in 6 K neon matrixes using a mass-selected C₁₀H₉⁺ ion beam. The absorption spectra reveal S₁/S₂ \leftarrow S₀ transitions with onsets at 502.1 and 396.1 nm for α -HN⁺, and 534.5 and 322.3 nm in the case of β -HN⁺. Wavelength-dispersed fluorescence was detected for α -HN⁺, starting at 504.4 nm. Light-induced α -HN⁺ \rightarrow β -HN⁺ isomerization was observed upon S₂ \leftarrow S₀ excitation of α -HN⁺, whereas β -HN⁺ relaxed back into the more stable alpha form either upon excitation to S₁ or via thermal population of the ground state vibrational levels near the top of the energy barrier between the two isomers. The intramolecular proton transfer leading to the α -HN⁺ \leftrightarrow β -HN⁺ photoisomerization is fully reversible. The observations are explained with the support of theoretical calculations on the ground- and excited states of the isomers, vertical excitation and adiabatic energies, minimum-energy pathways along the relevant reaction coordinates, and conical intersections between the electronic states.



1. INTRODUCTION

Protonated polycyclic aromatic hydrocarbons (H-PAH⁺s) are of interest from an astrophysical as well as a fundamental chemistry point of view. Among other polycyclic arene derivatives, H-PAH⁺s may play a role as intermediates toward soot formation in flames and combustion,^{1–3} and direct monitoring of such processes is possible once their electronic spectra have been observed. They are also known as intermediates in electrophilic aromatic substitution reactions.⁴

H-PAH⁺s have been the focus of investigations for over half a century with spectroscopic techniques and theoretical approaches; however, the information obtained was limited. The structure of, for instance, alpha- and beta-protonated naphthalenes (α - and β -HN⁺) has been shown by NMR in superacidic solutions to be a σ -complex of the excess hydrogen and the aromatic ring.^{5,6}

The topic of H-PAH⁺s has revived anew in context of astrophysical considerations. They have been proposed as carriers of unidentified infrared (UIRs) and perhaps diffuse interstellar (DIBs) bands.^{7–10} To follow up this hypothesis, their infrared and electronic spectra in the gas phase are needed. Several H-PAH⁺ cations have been studied in the gas phase using single- or multiphoton infrared dissociation and the spectra obtained were compared with UIRs.^{11–15} The gas-phase IR spectrum of the largest molecule studied so far, protonated coronene, resembles to some extent the UIR features.¹⁵

As for electronic spectroscopy, a few condensed-phase measurements are available.^{16–19} Recently, a number of H-PAH⁺s have been isolated in 6 K neon matrixes and their electronic spectra recorded.^{20–22} Two papers have appeared on

the electronic spectra of α -HN⁺ in the gas phase, reporting a single transition in the visible.^{23,24} The present study provides, apart from the system of α -HN⁺ above, also its second transition in the UV, as well as two electronic systems of β -HN⁺. Moreover, a reversible, photoinduced α -HN⁺ \leftrightarrow β -HN⁺ isomerization was observed and is explained with the support of theoretical calculations. This effect may induce new interest for H-PAH⁺s in the field of molecular electronics.^{25,26} Recent experimental studies show that light-induced hydrogen-transfer-based molecular switches are feasible.^{27,28}

2. EXPERIMENTAL SECTION

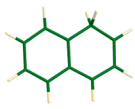
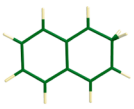
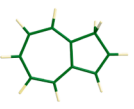
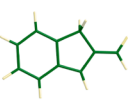
2.1. Production of Ions. Two methods were used for the generation of protonated naphthalenes. In the first, C₁₀H₉⁺ cations were produced from 1,2-dihydro-naphthalene (1,2-DHN) or 2-methyl-indene (2-MetI) in a hot-cathode discharge source. The fragment ion of $m/z = 129$ is one of the most intense in the mass spectrum of DHN obtained under such conditions. In the second, C₁₀H₉⁺ was generated in a proton transfer reaction (PT) between protonated methanol (MeOH₂⁺) and naphthalene (Naph) in the source. In the latter case and with a low MeOH pressure, both initial substances are ionized by electrons, and mainly their parent and fragment ions are formed (Figure S1A,B, green trace, Supporting Information). At higher pressures, the protonated species MeOH₂⁺ and HN⁺ start to form; further increase of the MeOH pressure leads

Received: October 26, 2012

Revised: December 16, 2012

Published: December 17, 2012

Chart 1. Structure and Relative Ground-State Energy (kJ mol^{-1}) of the Four Most Stable $\text{C}_{10}\text{H}_9^+$ Isomers and the Corresponding C_{10}H_9 Neutral Radicals (Parentheses) Obtained with DFT and MP2 Methods^a

				
	$\alpha\text{-HN}^+$	$\beta\text{-HN}^+$	1-HAz ⁺	2-IMe ⁺
DFT / B3LYP / cc-pVDZ	0 (0)	12 (20)	23 (97)	34 (15)
DFT / B3LYP / cc-pVTZ	0 (0)	12 (20)	24 (96)	33 (14)
MP2 / cc-pVDZ	0	16	9	33

^aOther possible geometries are shown in Chart S1 (Supporting Information).

to an efficient protonation of Naph. The HN^+ yield is higher than using the first method; moreover, the fragmentation is less pronounced.

As was previously demonstrated on protonated anthracene and larger H-PAH⁺s,²² the PT reaction ensures energetically milder conditions compared to the ionization and H loss of the respective dihydro-compounds, with preferential formation of the most stable H-PAH⁺ isomers. MeOH_2^+ was found to be the only suitable protonation agent of Naph among the reactants tested: H_3^+ , CH_5^+ , H_3O^+ , MeOH_2^+ , and protonated ethanol (EtOH_2^+), listed in the order of an increasing proton affinity (PA) of the corresponding neutral precursor.²⁹ Though in the case of EtOH_2^+ , the PT is energetically feasible (PA of EtOH is 779 kJ mol^{-1} and 803 kJ mol^{-1} for Naph),²⁹ no HN^+ was seen. A possible reason why HN^+ was not produced using the other proton donors is the large difference between their PAs and that of Naph; even if HN^+ was formed initially, the excess energy led to its dissociation. The optimal difference between the PAs of the proton donor and acceptor is $\sim 50 \text{ kJ mol}^{-1}$.

2.2. Matrix Isolation Spectroscopy. Electronic spectra of $\text{C}_{10}\text{H}_9^+$ were obtained using a mass-selective implementation of the matrix isolation technique.³⁰ Ions were generated from appropriate precursors (section 2.1), extracted from the source and guided through a deflector to separate them from neutral species, into a quadrupole mass filter. The $m/z = 129$ ion beam of 5–20 nA, selected at unity mass resolution, was codeposited with neon onto a rhodium-coated sapphire plate cooled by a closed-cycle helium cryostat to 6 K.

In order to efficiently trap the cations, chloromethane was mixed into the neon in a ratio of 1:20 000. CH_3Cl suppresses ion neutralization during deposition by capturing free electrons, thereby reducing the space charge in the matrix. To produce matrixes containing the highest concentration of neutral species with respect to cations, $\text{C}_{10}\text{H}_9^+$ ions were also trapped without admixture of an electron scavenger. In such experiments, most cations are neutralized with electrons ejected from metal surfaces, resulting in neutral species structurally identical with the cations.

Absorption spectra were recorded in the 220–1100 nm range by passing broadband light from a halogen or a high-pressure xenon lamp through the 20 mm long neon matrix. A bundle of optical fibers transmitted the light exiting the matrix to the entrance slit of a 0.3 m spectrograph equipped with range-specific CCD cameras. To eliminate the photoconversion of the trapped species by the broadband light used for the detection of spectra, cutoff filters were employed. Measurements were started at the longest wavelength and continued into the UV. The procedure was later repeated to test whether the species were light sensitive.

In the fluorescence studies, the matrix was irradiated using a pulsed, tunable laser with a bandwidth of $\sim 3\text{--}8 \text{ cm}^{-1}$ and $\sim 2\text{--}30 \text{ mJ}$ energy. The signal was collected, focused onto a bundle of quartz fibers, and transmitted to the spectrograph.³¹ Spectra were recorded in 50–65 nm wide overlapping sections with the same exposure time and number of accumulations for all spectral regions. The excitations were started from the lowest-energy absorptions and continued into the UV. The emission was measured starting 2 nm above the excitation wavelength to avoid the saturation of the CCDs with scattered laser light.

3. COMPUTATIONS

A number of $\text{C}_{10}\text{H}_9^+$ isomeric structures have been considered. A search for the most stable isomers was carried out using density functional theory (DFT) with the B3LYP functional³² and cc-pVDZ basis set.³³ The results are summarized in Chart S1 (Supporting Information). Vibrational frequencies were calculated to ensure that all these isomers are true minima on the $\text{C}_{10}\text{H}_9^+$ potential energy surface (PES). The four most stable $\text{C}_{10}\text{H}_9^+$ isomers are shown in Chart 1. The geometry of these was then reoptimized using a larger basis set, cc-pVTZ, as well as with the second-order Møller–Plesset perturbation theory (MP2)³⁴ at the cc-pVDZ level.

According to the DFT calculations and earlier results,^{7,11} the global minimum on the $\text{C}_{10}\text{H}_9^+$ PES is $\alpha\text{-HN}^+$. The other three isomers of Chart 1, $\beta\text{-HN}^+$, 1-azulenium (1-HAz⁺), and 2-indenylmethyl cation (2-IMe⁺), lie 13, 22, and 36 kJ mol^{-1} above it, respectively. The energetic order of $\beta\text{-HN}^+$ and 1HAz⁺ is reversed at the MP2/cc-pVDZ level: they are 16 and 9 kJ mol^{-1} higher than $\alpha\text{-HN}^+$. These four cations are planar with the exception of the CH_2 group, which lies in the plane perpendicular to the aromatic rings (C_s symmetry). Other possible $\text{C}_{10}\text{H}_9^+$ isomers are significantly higher in energy (Chart S1, Supporting Information) and were not considered further.

To support the assignment of the observed absorptions, excitation energies of the four most stable $\text{C}_{10}\text{H}_9^+$ isomers and their C_{10}H_9 neutrals were computed with time-dependent (TD) DFT and an ab initio second-order approximate coupled-cluster (CC2) method.^{35,36} In the latter case, the equilibrium geometry of the lowest-lying excited states was determined with CC2;³⁷ the preceding geometry optimization of the molecular systems in their ground electronic state was done with MP2 and the cc-pVDZ basis set.

In order to determine the barriers for the photophysically relevant reactions of α - and $\beta\text{-HN}^+$, minimum-energy profiles along the reaction coordinates in the ground S_0 and excited S_1 and S_2 states were determined by MP2 and CC2, respectively. After choosing a suitable coordinate value, all other nuclear

degrees of freedom were optimized in the construction of the path. The conical intersection (ConI) geometries between S_1 and S_0 for the two isomers were optimized with the complete active space self-consistent field (CASSCF) method³⁸ along with the cc-pVDZ basis set, with the active space comprising two electrons in two orbitals.

All MP2 and CC2 calculations were carried out with the Turbomole package,³⁹ using the resolution-of-the-identity approximation for the evaluation of the electron repulsion integrals.⁴⁰ The DFT, TDDFT, and CASSCF runs were done with routines in the Gaussian03 software.⁴¹

4. OBSERVATIONS

4.1. Visible Spectral Region. Deposition of $m/z = 129$ cations produced with either of the two described methods (section 2.1) into neon matrixes revealed several absorptions of different strength and bandwidth in the 250–700 nm range. Part of the spectrum recorded after deposition of mass-selected $C_{10}H_9^+$ ions produced in the reaction of Naph with $MeOH_2^+$ is characterized by an extended series of broad absorptions starting around 502 nm, as well as a weaker, narrower single band at ~ 528 nm (Figure 1, trace A). The former was not

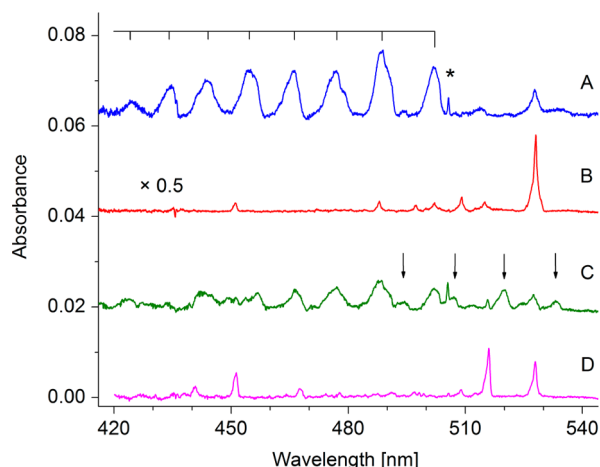


Figure 1. Electronic absorption spectra recorded in the visible after deposition of $C_{10}H_9^+$ cations produced from (A) a naphthalene/ $MeOH$ mixture and (C) 1,2-dihydro-naphthalene into a CH_3Cl /neon (1:20 000) matrix. Traces B and D were obtained from the same two precursors in experiments without an electron scavenger. All spectra were scaled to the same deposited charge of $C_{10}H_9^+$. Cationic bands are marked by their vibrational progression or arrows. Asterisk denotes C_2^+ , a common fragmentation product.

observed in an experiment without an electron scavenger in the neon host, whereas the latter was stronger (trace B). In trace B, several weak, sharper absorptions accompany the band at ~ 528 nm, which is the onset of this system. These weak features are not seen in trace A because they are hidden under the broad peaks. Deposition of $C_{10}H_9^+$ in a pure neon matrix led to efficient neutralization of the cations and formation of the neutrals, which maintained the cationic structure. Therefore, the 502 nm system originates from $C_{10}H_9^+$, whereas the one with an onset at 528 nm belongs to neutral $C_{10}H_9$.

The 502 nm system has also been observed, though weaker, when $C_{10}H_9^+$ was produced from 1,2-DHN and deposited into a neon matrix doped with CH_3Cl (Figure 1, trace C). Additionally, new absorptions commencing at 535 nm appeared. Both these systems were absent in the spectrum of

the $C_{10}H_9^+$ cations produced from the same precursor and deposited in a pure neon matrix. Two bands of neutrals at 528 and 516 nm dominate in this case. The former is identical with the system of $C_{10}H_9$ shown in trace B. The latter, which is unique for the 1,2-DHN precursor, is the band origin of another isomer of $C_{10}H_9$. Absorptions starting at 535 nm (trace C) are of cationic nature. The structure of this cation corresponds to the $C_{10}H_9$ neutral with band origin at 516 nm.

The use of 1,2-DHN as a precursor suggests the formation of two $C_{10}H_9^+$ isomers, α - and β - HN^+ , upon the removal of an H atom from one of the two CH_2 groups of the dihydrogenated molecule. These species should be responsible for the two cationic systems with onsets at 502 and 535 nm in the spectrum of $C_{10}H_9^+$ produced from 1,2-DHN (Figure 1, trace C). According to theoretical calculations (Chart 1), β - HN^+ lies ~ 16 kJ mol^{-1} higher in energy than α - HN^+ . Though 1-HAz $^+$ in the ground state has a similar energy to β - HN^+ , it can be excluded from further considerations on the basis of the large rearrangement of the precursor structure needed to form this ion. The prominent 502 nm system in the spectrum of $C_{10}H_9^+$ generated in the reaction of Naph with $MeOH_2^+$ is attributed to the most stable $C_{10}H_9^+$ isomer, α - HN^+ , because this method provides the mildest production conditions, as was shown on protonated pyrene.²² Consequently, the carrier of the 535 nm system is β - HN^+ . Several bands belonging to this absorption are distinguishable; they form a regular progression built on a ~ 490 cm^{-1} mode (Table 1).

Two papers on the electronic spectrum of jet-cooled α - HN^+ using photodissociation spectroscopy have recently appeared. The band origin of the $(1)^1A' \leftarrow \tilde{X}^1A'$ transition is reported at 503.36 nm in the gas phase,²⁴ in agreement with the neon matrix value of 502 nm. In the vibrational assignment of this system,²³ the most intense low energy modes (335 and 575 cm^{-1}) have counterparts in the spectrum of α - HN^+ in solid neon (Table 1).

Two $C_{10}H_9$ neutrals were formed in a pure neon matrix following neutralization of $C_{10}H_9^+$ generated from 1,2-DHN. The first system with an onset at 528 nm was the most prominent one obtained upon neutralization of α - HN^+ ; the second one starting at 516 nm is associated with the neutralization of β - HN^+ . These two neutral systems at 528 and 516 nm are the $D_1 \leftarrow D_0$ and $D_2 \leftarrow D_0$ transitions of α - and β -hydronaphthyl radicals (α - and β -HN), respectively; these are known from earlier studies on irradiated naphthalene crystals and solutions.^{42,43} They have also been observed in the gas phase by a mass-resolved resonant two-photon ionization technique.⁴⁴ In the latter paper, both neutral isomers were produced from 1,2-DHN, whereas only α -HN was seen from 1,4-dihydronaphthalene. Transitions of the two radicals overlap; they were separated and assigned by hole-burning spectroscopy and calculations. The onset of the $D_1 \leftarrow D_0$ transition of α -HN in the gas phase is at 527.7 nm. Several vibrational wavenumbers in the first excited electronic state were determined (e.g., 475, 564, 747, 965, and 1050 cm^{-1}); they are close to those derived for the 528 nm system in neon (Table S1, Supporting Information). The band origin of the β -HN system in the gas phase (516.4 nm) is spaced 412 cm^{-1} from that of α -HN; the separation is close to 448 cm^{-1} observed between the corresponding systems in a neon matrix. Thus, it is concluded that the α - and β -HN isomers are seen in the present study starting with the 1,2-DHN precursor, whereas only α -HN is apparent in the spectrum when the Naph/ $MeOH$ method was used. Furthermore, as the neutral $C_{10}H_9$ radicals

Table 1. Absorption Band Maxima ($\lambda_{\text{Ne}} \pm 0.1$ nm) of Electronic Transitions of $\text{C}_{10}\text{H}_9^+$ Cations Observed in 6 K Neon Matrixes and Assignment

λ_{Ne} (nm)	$\tilde{\nu}$ (cm^{-1})	$\Delta\tilde{\nu}$ (cm^{-1})	assignment ^a
$\alpha\text{-HN}^+$			
502.1	19 916	0	$0_0^0(1)^1\text{A}' \leftarrow \tilde{\text{X}}^1\text{A}'$
494.3	20 231	315	ν_{34}
488.0	20 492	576	ν_{31}
477.5	20 942	1026	ν_{26}
475.2	21 044	1128	ν_{24}
465.7	21 473	1557	ν_{11}
455.1	21 973	2057	$2\nu_{26}$
443.6	22 543	2627	$2\nu_{26} + \nu_{31}$
434.3	23 026	3110	ν_{47}
424.5	23 557	3641	$3\nu_{26}$
396.1	25 246	0	$0_0^0(2)^1\text{A}' \leftarrow \tilde{\text{X}}^1\text{A}'$
386.2	25 893	647	ν_{30}
377.1	26 518	1272	$2\nu_{30}$
$\beta\text{-HN}^+$			
534.5	18 709	0	$0_0^0(1)^1\text{A}' \leftarrow \tilde{\text{X}}^1\text{A}'$
520.8	19 201	492	ν_{32}
507.7	19 697	988	$2\nu_{32}$
495.4	20 186	1477	$3\nu_{32}$
483.8	20 670	1961	$4\nu_{32}$
472.2	21 177	2468	$5\nu_{32}$
322.3	31 028	0	$0_0^0(2)^1\text{A}' \leftarrow \tilde{\text{X}}^1\text{A}'$
317.8	31 467	439	ν_{32}
313.4	31 909	881	$2\nu_{32}$
309.1	32 348	1320	$3\nu_{32}$
305.0	32 789	1761	$4\nu_{32}$
2-Ime^+			
377.8	26 469	0	$0_0^0(2)^1\text{A}' \leftarrow \tilde{\text{X}}^1\text{A}'$
374.0	26 738	269	ν_{34}
371.2	26 940	471	ν_{32}
367.2	27 233	764	$\nu_{34} + \nu_{32}$ or ν_{29}
364.8	27 412	943	$2\nu_{32}$ or ν_{26}
362.9	27 556	1087	ν_{24}
360.1	27 770	1301	$\nu_{34} + \nu_{24}$ or ν_{19}
357.2	27 996	1527	2×764
355.8	28 106	1637	$\nu_{9/10}$
352.1	28 401	1932	

^aVibrational assignments in the excited states of $\text{C}_{10}\text{H}_9^+$ are based on ground-state fundamentals calculated with DFT at the B3LYP/cc-pVTZ level of theory and listed as footnote a of Table 3 for $\alpha\text{-HN}^+$ and in Table S2 (Supporting Information) for the other three isomers of Chart 1.

formed by the neutralization of $\text{C}_{10}\text{H}_9^+$ in the matrix retain the cationic structure, the identification of the spectral features of α - and β -HN corroborates the assignment of the 502 and 535 nm systems to the α - and β -HN⁺ isomers, respectively.

4.2. UV Spectral Region. The UV part of the absorption spectrum recorded after the deposition of mass-selected $\text{C}_{10}\text{H}_9^+$ ions, produced in the reaction of Naph with MeOH_2^+ , into a neon matrix containing CH_3Cl shows strong absorptions in the 250–400 nm region (Figure 2, trace A). The spectrum obtained when the ions were produced from the same precursor and deposited into a matrix without an electron scavenger is simpler (trace C). Three electronic systems with onsets at 369, 331, and 324 nm are seen (Table S1, Supporting Information). They are due to neutral α -HN because they were observed in the same matrix as its 528 nm system. Moreover,

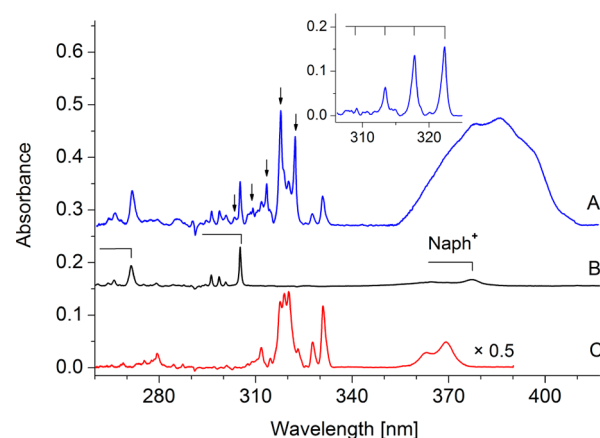


Figure 2. UV part of the absorption spectra recorded after deposition of $\text{C}_{10}\text{H}_9^+$ cations produced from naphthalene/MeOH (A) with and (C) without an electron scavenger in neon. The spectra were normalized to the same accumulated charge of $\text{C}_{10}\text{H}_9^+$. Bands due to naphthalene radical cation (Naph^+) are seen in trace A; trace B is part of the Naph^+ spectrum recorded in another experiment (Figure S2, Supporting Information), scaled to the same intensity as the origin band at ~ 670 nm. The inset shows the $\text{S}_2 \leftarrow \text{S}_0$ transition of β -protonated naphthalene obtained by subtracting trace C from trace A after proper intensity scaling; these same absorptions are also marked by arrows on trace A.

their relative intensities correlate with that of the α -HN system in the visible in different experiments and precursors used. The absorptions of neutral α -HN are also present in trace A as a result of partial neutralization of the cations during the growth of the matrix. Besides these, absorptions of naphthalene cation (Naph^+) weakly contribute to the spectrum (Figure 2, trace A). They are shown in trace B, which is a UV section of the pure Naph^+ spectrum (Figure S2, Supporting Information), down-scaled to the intensity of its band origin (~ 670 nm) observed after deposition of $\text{C}_{10}\text{H}_9^+$. Naph^+ is present in the matrix because its ^{13}C isotopologue has the same mass as HN^+ . The fragmentation of HN^+ during matrix growth could be a second reason. The remaining absorptions, a broad one centered at 385 nm and a system of sharp bands starting at 322 nm (Figure 2, trace A), belong to the HN^+ cations.

HN^+ has been studied in acidic solutions by absorption spectroscopy. In such media, the spectrum of HN^+ is characterized by a strong, broad absorption around 390 nm, which has later been assigned to $\alpha\text{-HN}^+$.^{17,19} The 385 nm system of $\text{C}_{10}\text{H}_9^+$ observed in neon (Figure 2, trace A) is similar to that. The intensity of this band may be slightly overestimated due to an experimental background artifact in this region. The band is ~ 40 nm broad, with a barely discernible vibrational structure (Table 1). This suggests a short lifetime of the cation in this excited electronic state. A broad absorption was also reported for the $\text{S}_1 \leftarrow \text{S}_0$ transition of protonated benzene in a neon matrix,²⁰ which, according to calculations,⁴⁵ can be associated with a fast decay of S_1 to S_0 via a conical intersection.

The other cationic system with an origin at 322 nm (marked with arrows in Figure 2, trace A) is well pronounced. It is seen even better in the inset of Figure 2, for which the spectrum recorded in pure neon (trace C) was subtracted from that doped with CH_3Cl (trace A) after downscaling the former to the same intensity of the 331 nm band of the neutral on the latter. Five narrower bands constitute the 322 nm system and form a vibrational progression in a ~ 440 cm^{-1} mode (Table 1).

It could be expected that the two cationic absorption systems in the UV originate from α -HN⁺ because its transition dominates the visible part of the spectrum measured in the same matrix (Figure 1, trace A). These belong, however, to two different isomers of C₁₀H₉⁺ because their relative intensities vary with the experimental conditions. The 385 nm system is attributed to the α -HN⁺ isomer, whereas the one with an onset at 322 nm originates from β -HN⁺, as is elucidated further in sections 4.3 and 4.4.

TDDFT and CC2 calculations predict that the two lowest-energy electronic states (S₁ and S₂) of α -HN⁺ and β -HN⁺ have $^1(\pi, \pi^*)$ character. Vertical excitation energies calculated for the ground-state geometry of the cations are overestimated by 0.3–0.5 eV with respect to the neon matrix data (Table 2). The

Table 2. Excited-State Symmetries, Vertical Excitation Energies ΔE^{VE} , and Oscillator Strengths f for the Three Observed C₁₀H₉⁺ Isomers and Respective C₁₀H₉ Neutrals Calculated with Two Methods, and Comparison with Experimental Data^a

exc. state	TD DFT//B3LYP/ cc-pVTZ		CC2//MP2/cc- pVDZ		exptl ^b (eV/nm)
	ΔE^{VE} (eV)	f	ΔE^{VE} (eV)	f	
α -HN ⁺ , \tilde{X}^1A'					
$^1A'$ ($\pi\pi^*$)	2.86	0.020	2.95	0.037	2.47/502
$^1A'$ ($\pi\pi^*$)	3.60	0.25	3.48	0.32	3.13
$^1A''$ ($\sigma\pi^*$)	4.75	0.0007	5.08	0.0009	
β -HN ⁺ , \tilde{X}^1A'					
$^1A'$ ($\pi\pi^*$)	2.78	0.074	2.73	0.11	2.32/535
$^1A'$ ($\pi\pi^*$)	4.36	0.075	4.42	0.17	3.85
$^1A'$ ($\pi\pi^*$)	4.53	0.012	4.63	0.011	
2-Ime ⁺ , \tilde{X}^1A'					
$^1A'$ ($\pi\pi^*$)	2.82	0.017	2.95	0.025	
$^1A'$ ($\pi\pi^*$)	3.83	0.55	3.68	0.66	3.28
$^1A'$ ($\pi\pi^*$)	5.03	0.028	5.17	0.033	
α -HN, \tilde{X}^2A''					
$^2A'$	2.81	0.0021	3.45	0.0011	2.35
$^2A'$	3.13	0.0019	4.05	0.0010	3.36
$^2A'$	3.63	0.022	4.57	0.28	3.75
$^2A'$	3.80	0.19	4.65	0.0005	3.87
$^2A'$	4.06	0.0033	4.71	0.028	
$^2A''$	4.46	0.0014			
β -HN, \tilde{X}^2A''					
$^2A'$	2.43	0.0012	3.29	0.0008	
$^2A'$	3.15	0.052	3.93	0.0009	2.40
$^2A'$	3.33	0.0024	4.12	0.081	
$^2A'$	3.59	0.0001			
$^2A'$	4.23	0.030			
$^2A'$	4.60	0.020			
2-Ime, \tilde{X}^2A''					
$^2A'$	2.89	0.015	3.46	0.026	2.75
$^2A'$	3.21	0.0018	4.10	0.0025	
$^2A'$	3.59	0.016	4.59	0.084	4.36
$^2A'$	4.00	0.039	4.63	0.070	
$^2A'$	4.28	0.40			

^aComputational results for the fourth cationic and neutral isomers of Chart 1; 1-HAz⁺ and 1-HAz, are listed in Table S3 (Supporting Information). ^bOrigin band positions in neon matrixes of this study (see Tables 1 and S1, Supporting Information).

agreement is better comparing these latter with the adiabatic excitation energies, where geometries of both states involved in the transition were optimized. The calculation predicts also the right order of the electronic systems in the spectra of these cations. In the visible range, β -HN⁺ absorbs at longer wavelengths than α -HN⁺, whereas in the UV it is the reverse. Moreover, the calculated oscillator strengths qualitatively agree with the observed relative intensities of the S₁ \leftarrow S₀ and S₂ \leftarrow S₀ transitions. The f value of the UV transition of α -HN⁺ is an order of magnitude larger than its visible one, whereas similar values for the UV and visible systems are predicted for β -HN⁺. The visible and UV systems of α - and β -HN⁺ have been assigned according to the theoretical calculations to their (1)¹A' \leftarrow \tilde{X}^1A' and (2)¹A' \leftarrow \tilde{X}^1A' transitions, respectively.

Besides the absorptions of the two HN⁺ isomers and their neutral species, another cationic system is present in the spectrum of C₁₀H₉⁺ produced from 1,2-DHN. This feature at 378 nm is imposed on the broad UV absorption of α -HN⁺ (Figure 3). Several relatively sharp bands contribute to this

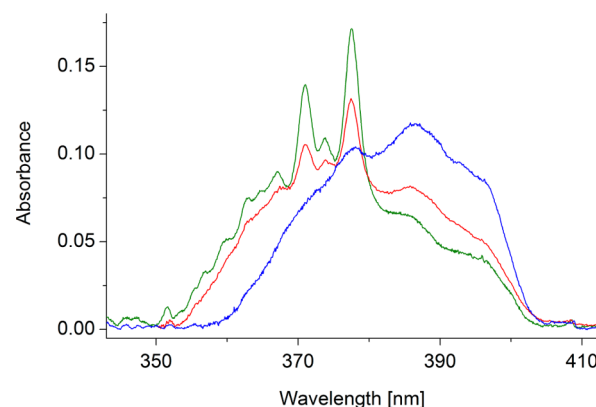


Figure 3. Part of the absorption spectrum of C₁₀H₉⁺ produced from a naphthalene/MeOH mixture (blue trace), 1,2-dihydro-naphthalene (red), and 2-methyl-indene (green) and deposited in a neon matrix doped with CH₃Cl. The spectra were normalized to the same accumulated charge of C₁₀H₉⁺. The S₂ \leftarrow S₀ transitions of α -protonated naphthalene and 2-indenylmethylum overlap (see text).

system (Table 1). Other than α - and β -HN⁺, two low-energy isomers of C₁₀H₉⁺ are considered as candidates of these absorptions; these are 1-HAz⁺ and 2-Ime⁺ (Chart 1). Experimental studies on C₆H₇⁺ isomers (whose benzene-fused analogues are, among others, the HN⁺s) pointed out the presence of α -protonated fulvene as the isomer nearest in energy to protonated benzene.^{46–48} Both protonated benzene and α -protonated fulvene were simultaneously trapped in solid neon under similar experimental conditions as here.²⁰ Moreover, it was proven that topomerization of naphthalene proceeds through benzofulvene as an intermediate step, which needs the rearrangement of a benzene ring. It can also be expected then that the 1,2-DHN precursor of C₁₀H₉⁺ or the cations themselves rearrange in the ion source leading to the protonated benzofulvene cation 2-Ime⁺.

To test whether the 378 nm absorption system belongs to the benzofulvenic isomer of C₁₀H₉⁺, the m/z = 129 cations produced from 2-MetI were deposited into a neon matrix doped with CH₃Cl. The spectrum obtained was similar to that using 1,2-DHN; however, the 378 nm band was stronger and all spectral features of α - and β -HN⁺ were much weaker (Figure

3, blue trace). The spectra shown are normalized to the same deposited charge.

Calculations predict that 2-IME⁺ is the most stable structure of C₁₀H₉⁺ among those with an indene skeleton (Chart S1, Supporting Information). It can be formed from the 2-MeI precursor by a simple H loss from the methyl group. 1HAz⁺ is even lower in energy than 2-IME⁺; however, its production from the indene-based precursor is less probable, as it would involve rearrangement of a six-membered ring breaking its aromatic stability. Calculations predict a weak (1)¹A' ← \tilde{X}^1 A' transition of 2-IME⁺ in the visible range and ~50 times stronger (2)¹A' ← \tilde{X}^1 A' in the UV (Table 2). The intensity of the first transition of 2-IME⁺ was too low to be observed.

Photobleaching of the C₁₀H₉⁺ cations produced from 1,2-DHN led to the increase of the α -HN and β -HN features, as well as to the appearance of new systems with origins at 451 and 284 nm. The latter two were even stronger after the UV irradiation of C₁₀H₉⁺ produced from 2-MeI; therefore, they are assigned to the 2-IME neutral radical. The wavelengths of the bands, with their vibrational assignment based on the calculated energies of the normal modes in the ground state of this radical are given in Table S1 (Supporting Information).

4.3. Fluorescence. Fluorescence measurements were carried out on a matrix containing C₁₀H₉⁺ produced in the Naph/MeOH₂⁺ reaction. Laser excitation into any of the absorption bands of the 502 nm system of α -HN⁺ resulted in a structured emission in the 504–625 nm region. The spectrum is shown in Figure 4, red trace, along with the corresponding

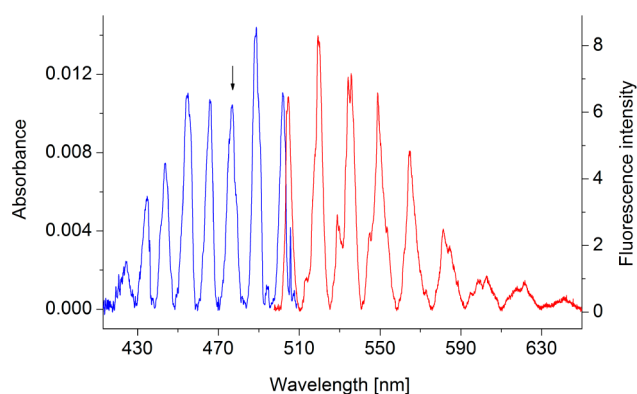


Figure 4. Absorption (blue trace) and fluorescence (red) spectra recorded after deposition of C₁₀H₉⁺ cations produced from a naphthalene/MeOH mixture. The emission was obtained upon excitation of the 477.5 nm absorption feature (arrow). The two spectra cross at 503.5 nm, the zero-phonon line of the absorption and emission.

absorption scan (blue). The vibrational structure of the fluorescence is a mirror image of the absorption bands and the onsets of the two spectra partially overlap and cross at 503.5 nm, the position of their zero-phonon lines. This is also a more precise energy for the 0₀⁰ band of the S₁ ← S₀ transition of the α -HN⁺ isomer in a neon matrix. The band origin in neon is shifted ~10 cm⁻¹ to the red from the gas-phase value.^{23,24} The 504 nm fluorescence system, though much weaker in intensity, was also detected upon excitation in the 370–396 nm range, where the strong, broad absorption of α -HN⁺ is located. The observations of the same fluorescence spectrum indicate that the 502 and 385 nm systems belong to the same isomer, α -HN⁺.

The wavelengths of the fluorescence band maxima are given in Table 3. The spectrum is similar to the 502 nm absorption

Table 3. Fluorescence Band Maxima ($\lambda_{\text{Ne}} \pm 0.1$ nm) and Vibrational Assignment of the S₁ → S₀ Transition of Alpha-Protonated Naphthalene in a 6 K Neon Matrix

λ_{Ne} (nm)	$\tilde{\nu}$ (cm ⁻¹)	$\Delta\tilde{\nu}$ (cm ⁻¹)	assignment ^a
504.4	19 826	0	0 ₀ ⁰ (1) ¹ A' → \tilde{X}^1 A'
512.7	19 505	321	ν_{34}
517.6	19 320	506	ν_{33} or ν_{32}
520.1	19 227	599	ν_{31}
528.8	18 911	915	$\nu_{34} + \nu_{31}$ or ν_{28}
529.9	18 871	955	ν_{27}
534.1	18 723	1103	$\nu_{33} + \nu_{31}$ or ν_{25}
535.8	18 664	1162	ν_{24}
544.8	18 355	1471	ν_{14}
548.9	18 218	1608	ν_{10}
550.4	18 169	1657	ν_9
551.8	18 123	1703	$\nu_{31} + 1103$
553.6	18 064	1762	$\nu_{31} + \nu_{24}$
564.5	17 715	2111	$\nu_{27} + \nu_{24}$
572.9	17 455	2371	$\nu_{14} + 915$
581.1	17 209	2617	$\nu_{27} + \nu_9$
584.7	17 103	2723	$\nu_{10} + 1103$
594.7	16 815	3011	ν_8
598.4	16 711	3115	ν_7
602.8	16 589	3237	ν_1
621.8	16 082	3744	$\nu_{33/32} + \nu_1$

^aThe assignments are based on the totally symmetric (a' in C_s) modes in the electronic ground state of α -HN⁺ calculated with DFT at the B3LYP/cc-pVTZ level of theory (unscaled): 3222, 3221, 3207, 3199, 3194, 3192, 3182, 2981, 1663, 1613, 1590, 1546, 1493, 1463, 1438, 1406, 1370, 1313, 1290, 1259, 1211, 1187, 1181, 1150, 1109, 1050, 974, 922, 796, 751, 607, 502, 501, and 355 cm⁻¹.

system. Both contain a weak band spaced by 321 and 315 cm⁻¹ from the origin, respectively. This is followed by the second peak, strongest in both spectra, located ~580–590 cm⁻¹ from the origin. The third emission feature consists of at least four overlapping bands, 915, 955, 1103, and 1162 cm⁻¹, and may explain the slight asymmetry of some of the absorption bands. The vibrational structure in the fluorescence maps out some of the vibrational energy levels in the ground electronic state. These can be compared directly to the calculated energies of the vibrational normal modes in the ground state of α -HN⁺ (Table 3, footnote a). No fluorescence features were detected upon laser excitation across the 535 and 322 nm absorption systems.

4.4. α -HN⁺ ↔ β -HN⁺ Photoisomerization. Repeating the scans in the visible region after measurements in the UV revealed changes in the absorption spectrum of C₁₀H₉⁺ produced in the reaction of Naph with MeOH₂⁺. The intensity of the 502 nm system of α -HN⁺ lowered and the 535 nm system appeared (Figure 5, traces A and B), the latter being identical to the one produced from 1,2-DHN (Figure 1, trace C) and assigned to β -HN⁺. Prolonged photolysis with UV photons of a high-pressure xenon lamp equipped with a band-pass filter, transmitting the light 340 < λ < 390 nm where the strong broad absorption of α -HN⁺ is located, fully depleted the 502 nm system of this cation and resulted in the further growth of the 535 nm one of β -HN⁺ (Figure 5, trace C). However, repetition of the scans in the visible region caused each time a

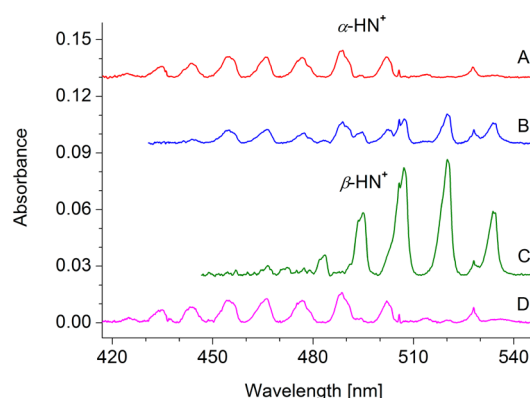


Figure 5. Absorption spectra of α - and β -protonated naphthalenes illustrating the observed photophysical processes. Visible part of the spectrum of $C_{10}H_9^+$ cations produced from naphthalene/MeOH mixture recorded after (A) deposition into a neon matrix with electron scavenger, (B) measurement in the UV region, (C) subsequent 20 min irradiation with $340 < \lambda < 390$ nm using a high-pressure xenon lamp, and (D) 10 min, $\lambda > 508$ nm bleaching by a halogen lamp.

gradual decrease of the bands of β - HN^+ and a steady increase of the 502 nm system of α - HN^+ . The spectrum shown in Figure 5, trace C, was recorded just after a 20 min, $340 < \lambda < 390$ nm UV irradiation of the matrix using the shortest possible exposure time and only a few accumulations, thus corresponding to the maximum amount of β - HN^+ in the matrix and no α - HN^+ .

A 10 min exposure of the matrix containing only β - HN^+ (when the 535 nm system was strong and the spectrum was as in Figure 5, trace C) to $\lambda > 508$ nm filtered light of a halogen lamp depleted the absorptions of β - HN^+ completely, whereas the 502 nm system of α - HN^+ became strong (Figure 5, trace D). It is identical to that in trace A; thus, the α - $HN^+ \leftrightarrow \beta$ - HN^+ photoisomerization is a reversible process. Further tests showed that the cations survive in the matrix by virtually any back-and-forth photoconversion cycles induced by the UV and visible irradiations at wavelengths $340 < \lambda < 390$ nm and $\lambda > 508$ nm, respectively.

To elucidate the behavior of the UV bands of $C_{10}H_9^+$ upon such irradiations and their relation to the absorption systems in the visible, systematic studies were carried out. Matrixes were

irradiated first with photons of appropriate wavelength to fully convert $C_{10}H_9^+$ to either the α - or the β - HN^+ isomer. Next, a set of stepwise exposures with $340 < \lambda < 390$ nm or $\lambda > 508$ nm was undertaken. The subsequent scans were restricted only to the visible and UV regions where the absorptions of the HN^+ isomers occur. These spectra were measured using a set of cutoff and band-pass filters; furthermore, the number of accumulations was drastically reduced, all in order to prevent the photoconversion of the isomers during recording the spectra.

Figure 6A,B illustrate the photoinduced transformation situation between α - $HN^+ \leftrightarrow \beta$ - HN^+ as regards to the correlation of their visible and UV systems. First, HN^+ was produced in the reaction of Naph with $MeOH_2^+$ and the matrix irradiated for 10 min with $\lambda > 508$ nm to convert all HN^+ into α - HN^+ . The strong 502 nm system was observed as in Figure 5, trace D, and the spectrum was then measured in the 300–420 nm range (Figure 6B, red trace). After this scan, the visible range was also recorded (Figure 6A, red trace). The absorptions of β - HN^+ with an onset at 535 nm are already present due to the photoconversion of α - HN^+ to β - HN^+ caused by the UV light used for recording the spectrum. Next, the matrix was exposed for 12 min to the $340 < \lambda < 390$ nm photons and the same ranges were remeasured (Figure 6A,B, blue traces). The systems of α - HN^+ (that at 502 nm and the broad one around 385 nm) became weaker, whereas the 535 nm system of β - HN^+ , together with the sharper commencing at 322 nm, grew in intensity. In the subsequent step, the matrix was irradiated for another 20 min with $340 < \lambda < 390$ nm light, and the spectrum was recorded (green traces in Figure 6B,A). Changes in the spectrum of HN^+ upon this second photolysis step were more pronounced than those caused by the previous irradiation. The broad 385 nm system of α - HN^+ diminished, whereas the 502 nm absorption was eliminated. Although this latter system was not to be seen, this is probably due to the low oscillator strength of the 502 nm transition because the (weak) presence of the system at 385 nm suggests that some α - HN^+ was still in the matrix. The absorptions at 535 and 322 nm behave in a similar way upon photolysis: both are produced by prolonged irradiation of the 385 nm system of α - HN^+ and decay when irradiated with $\lambda > 508$ nm light producing back

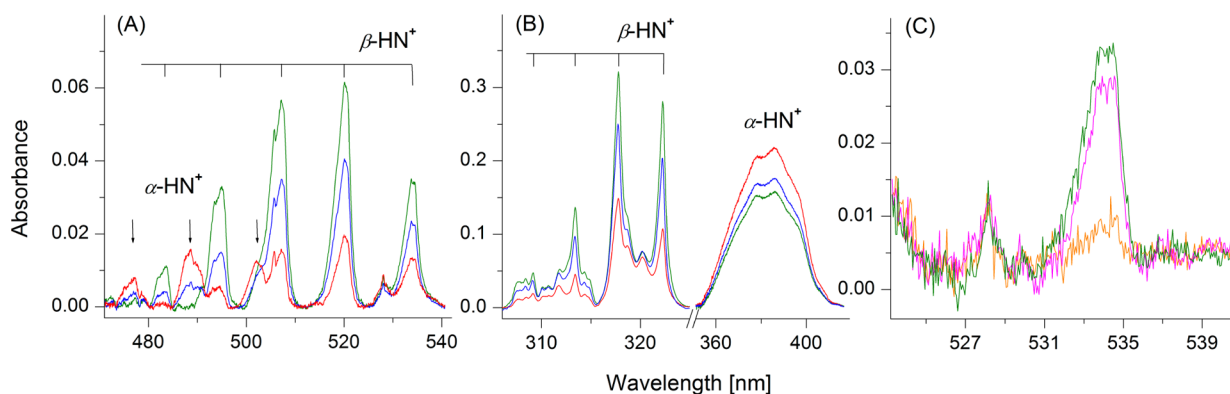


Figure 6. Absorption spectra of α - and β -protonated naphthalenes illustrating the observed photophysical processes. Panel A: Visible section of the spectra of $C_{10}H_9^+$ cations produced from a naphthalene/MeOH mixture, recorded after UV measurements (red trace) and subsequent 12 (blue) and 20 min (green) bleaching of the matrix with $340 < \lambda < 390$ nm radiation. Panel B: UV region measured reproducing the irradiation conditions used in panel A. Panel C: Origin band region of the 535 nm absorption system of β -protonated naphthalene recorded using cutoff filters blocking the light below ~ 520 nm. The green and magenta traces were measured in a ~ 2 min sequence to illustrate the intensity decay caused by the light used for recording the spectra, whereas the orange curve was recorded after the matrix was left in darkness for ~ 30 min.

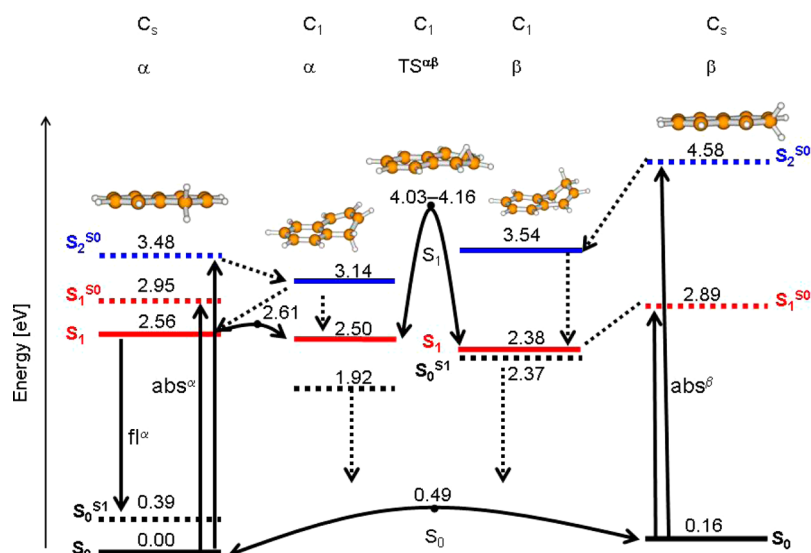


Figure 7. Vertical (dashed lines) and adiabatic (solid) energies for the $S_1 \leftarrow S_0$ and $S_2 \leftarrow S_0$ transitions of α - and β -protonated naphthalenes. Ground-state energy computed at the optimized geometry of the first excited-state minimum is denoted as S_0^{S1} . The energy (eV) of a given state is relative to the global minimum (S_0 of α -HN $^+$). Absorption “abs” and fluorescence “fl” processes observed are indicated by solid lines, whereas the internal conversion by dashed ones. TS $^{\alpha\beta}$ denotes the transition state between the α - and β -HN $^+$ isomers. Energy barriers between the respective states are shown with arrows at each end.

the absorptions of α -HN $^+$. Therefore, they are of common origin and belong to β -HN $^+$.

Besides the reversible α -HN $^+ \leftrightarrow \beta$ -HN $^+$ photoisomerization, decay of β -HN $^+$ was also observed when the matrix containing this cation was left for 30 min in the dark. Figure 6C shows the origin band of the 535 nm system recorded using filters, which block the light below ~ 520 nm. The green and magenta traces were measured right after each other; the comparison of their intensity shows that there is only a modest change caused by the exposure to the light used for the absorption measurements. The orange trace was recorded after the matrix was left in the dark for 30 min; the 535 nm origin band of β -HN $^+$ almost completely depleted in this case.

Calculations (section 5) show that β -HN $^+$ requires about 2600 cm^{-1} to overcome the barrier of a $\beta \rightarrow \alpha$ proton shift in the ground electronic state. At the neon matrix temperature of 6 K, only ca. 4×10^{-14} of all the cations are in the lowest excited vibrational level lying $\sim 100\text{ cm}^{-1}$ above the zero-point energy; thus, quantum tunneling from the zero vibrational level of β -HN $^+$ could be considered to describe the observed phenomenon. Similar processes have been inferred to take place in low-temperature matrixes, among others, for the *cis/trans* isomerism of formic acid HCOOH investigated by IR 49,50 or for the deuterium scrambling in substituted methane radical cations using electron spin resonance. 51,52

Another, more plausible explanation is the following. In our setup, the matrix is not completely shielded thermally from the surrounding metal parts, which are at room temperature. As a result, β -HN $^+$ trapped in the matrix may absorb some blackbody radiation; the photons of energy $2000\text{--}600\text{ cm}^{-1}$ from the high-energy edge of the blackbody spectrum (0.3% of the total at 300 K) excite then the cations and cause the proton shift near the top of the isomerization barrier.

5. THEORETICAL STUDIES ON ELECTRONIC STATES AND PHOTOPHYSICS OF HN $^+$

Unrestrained optimization of the ground electronic state of α - and β -HN $^+$ with the CC2/cc-VDZ method leads to two stable,

planar forms as shown in Chart 1. The β -HN $^+$ isomer, ~ 0.16 eV higher in energy, is separated from α -HN $^+$ by a barrier of ~ 0.33 eV (Figure 7). Vertical excitation energies for the two lowest excited singlet states S_1 and S_2 , computed for both cations at their ground-state equilibrium geometry, are indicated in Figure 7 by horizontal dashed lines S_1^{S0} (red) and S_2^{S0} (blue) and the transitions by black vertical arrows. The energies and oscillator strengths of these transitions are given in Table 2.

The energy landscape of the excited states of HN $^+$ is more complex than that of S_0 . Optimization of the S_1 state of HN $^+$ in C_s symmetry starting from the ground-state equilibrium geometries leads to a stable minimum for α -HN $^+$, located 2.56 eV above the global minimum, S_0 of α -HN $^+$ (red solid line in Figure 7). The S_1 state of β -HN $^+$ is predicted 2.57 eV above S_0 of α -HN $^+$ (Table 4); however, it is unstable with respect to the out-of-plane deformation of the CH_2^+ moiety and thus is not shown in Figure 7.

The unrestrained optimization (in C_1 symmetry) of the first excited state of β -HN $^+$ results in the fulvene-like structure of

Table 4. Energies (in eV, Relative to S_0 of α -HN $^+$) at Equilibrium Geometries of the S_0 , S_1 and S_2 States of α - and β -HN $^+$ Obtained with the CC2/cc-pVDZ Method; Values for the Other States Are Denoted with Sub- and Superscripts (e.g., S_0^{S1} Is the Energy of S_0 Calculated at S_1 Geometry)

	C_s^α	C_1^α	C_1^β	C_s^β
S_0	0.			0.16
S_0^{S1}	0.39	1.92	2.37	0.49
S_0^{S2}	0.26	0.67	2.75	0.35
S_1	2.56	2.50	2.38	2.57 ^a
S_1^{S0}	2.95			2.89
S_1^{S2}	2.86	2.99	2.97	2.75
S_2	3.25 ^a	3.14	3.54	4.39 ^a
S_2^{S0}	3.48			4.58

^aUnstable upon C_s symmetry breaking.

2.38 eV energy. The corresponding prefulvenic geometry of α -HN⁺ was also found. Its energy, 2.50 eV relative to the global minimum of the cations, is slightly lower than that of the S₁ state of α -HN⁺ in C_s symmetry (Figure 7). These two S₁ minima of α -HN⁺ at 2.56 and 2.50 eV are separated by a small, \sim 0.05 eV energy barrier. It can thus be concluded that the (broadband) excitation of α -HN⁺ to its S₁ state may result in the population of either the planar or the prefulvenic structure, whereas the S₁ excitation of the β -HN⁺ isomer leads to its nonplanar form only.

The interatomic distance between the two carbon atoms adjacent to the CH₂⁺ moiety is significantly shorter in the two prefulvenic forms than in the planar structures. The energies of the ground state of α - and β -HN⁺ calculated for the S₁ equilibrium geometries (S₀^{S1}) are significantly higher for the prefulvenic structures than at the planar geometries, and as a consequence, there is a drastic reduction in the S₁–S₀ energy gaps. This amplifies nonadiabatic coupling and induces an efficient internal conversion to the ground state (vertical dashed black arrows, Figure 7). After an excitation to S₁, once either of the cations reaches again the ground state PES by relaxation, their thermal energy will be much larger than the barrier separating the two isomers. Therefore, irrespective of in which prefulvenic structure (α or β) in the S₁ state the internal conversion starts, it will lead to a mixture of the two isomers of HN⁺. Though the energy difference between the S₁ prefulvenic structures of α - and β -HN⁺ is relatively small, they are separated by a high, \sim 1.5 eV barrier, and the cations cannot isomerize on the S₁ PES.

The second excited singlet states were also calculated independently for both cations. The C_s symmetry-restricted optimization of S₂ provides the adiabatic electronic excitation energies of α - and β -HN⁺ as 3.25 and 4.39 eV, respectively (Table 4); however, both isomers have an imaginary out-of-plane vibration in the CH₂⁺ unit. The S₂ states at this planar geometry thus have no physical meaning and are not indicated in Figure 7. Unconstrained optimization results in two stable prefulvenic minima of energy 3.14 and 3.54 eV for α - and β -HN⁺, respectively. The proximity (0.64 eV) of the S₂ and S₁ levels of α -HN⁺ in the prefulvenic geometry will cause fast relaxation of α -HN⁺ from the S₂ state to the near lying S₁; this process is indicated by the vertical dashed arrow (Figure 7). α -HN⁺ excited to its S₂ state can also relax to S₁ of the planar structure; this leads to a weak fluorescence (section 4.3). The fast decay of the S₂ state can explain the broadness in the UV absorption band of α -HN⁺ (Figure 2). The corresponding S₂–S₁ energy difference for β -HN⁺ is 1.16 eV; the cation lives much longer in the S₂ state than one vibrational period, and the mode pattern is well discernible in its UV spectrum.

The small S₁–S₀ energy gaps for the prefulvenic structures of α - and β -HN⁺ suggest that the S₁ → S₀ internal conversion is efficient. Although the CC2 approach, a single-reference method, is unable to locate precisely and characterize the ConI between these states, it foretells the presence of a ConI in the vicinity of the CC2 optimized geometry. A CASSCF search for the lowest-energy ConI between the S₁ and S₀ states starting from the CC2 optimized geometries of α - and β -HN⁺ in the S₁ state (C₁ symmetry) resulted in locating the chairlike ConI ^{α} and ConI ^{β} structures (Figure S3, Supporting Information). Both of these have the same motif: the beta carbon distorted out of the molecular plane, irrespective of the position of the proton (α or β).

The minima of two prefulvenic structures are separated from each other by a sizable barrier of about 1.5 eV on the S₁ PES (Figure 7). This practically precludes a PT to take place between them in the S₁ state, even considering the excess energy available from the excitation to S₂. This is in contrast to the situation in the ground state where the two isomers are separated by a much smaller barrier. An explanation is that, in the S₀ state, the excess proton interacts with the neutral molecular frame and can easily jump between carbon atoms. The S₁ ← S₀ excitation of HN⁺ shifts the positive charge from the CH₂⁺ moiety to the ring of the cation, as can be seen from the inspection of the molecular orbitals involved (Figure S3, Supporting Information). As a result, the CH₂ group gets an alkane-like character, and a transformation of one isomer into another would involve the breaking and formation of (partially) covalent CH bonds, which is reflected by the high barrier on the S₁ PES.

The following photophysical scheme of HN⁺ emerges. α -HN⁺ in the S₁ state can exist in two isoenergetic structures, planar and nonplanar, separated by a low energy barrier (Figure 7). Its optical excitation from S₀ to near the bottom of the S₁ state results in fluorescence because this local minimum is protected by a barrier from the S₁/S₀ conical intersection ConI ^{α} . At higher-energy excitation to this state or due to an excitation within the S₂ manifold, access to ConI ^{α} opens, and the system may return to the ground state in a radiationless way with lower probability of emission from the local minimum of the S₁ state. In the case of β -HN⁺, there is no stable minimum on the S₁ PES near the Franck–Condon geometry, which could be protected by a barrier from the abyss of the ConI with the ground state. The relaxation of this planar geometry to its ConI ^{β} form is exothermic by about 0.5 eV. Thus, β -HN⁺ is not expected to fluoresce from S₁ for neither planar nor nonplanar structures as both these are subject to fast nonradiative relaxation to the ground electronic state. In other words, β -HN⁺ deactivates optical excitation via the radiationless pathway through the S₁/S₀ conical intersection, whereas fluorescence can be observed only from the S₁ state of the planar structure of α -HN⁺.

Inspection of Figure 7 suggests that, although the PT process in the S₁ state is unlikely to occur in view of a large barrier separating the cations, such reaction can take place on the ground-state PES because this state is populated with excess of vibrational energy due to the S₁ → S₀ internal conversion at the ConIs. The energy is sufficient to overcome the ground-state barrier and the system can end up at a ground-state minimum of the initial cation or can flow toward the minimum of the other isomer of HN⁺. The photoinduced isomerization mechanism sketched above is similar to that suggested previously for protonated benzene.⁴⁵

6. CONCLUSIONS

Three isomers of C₁₀H₉⁺ (α - and β -HN⁺ and 2-Ime⁺) have been produced by ionizing fragmentation of 1,2-DHN, whereas only α -HN⁺ (the most stable one) was formed in a proton transfer reaction between MeOH₂⁺ and naphthalene. The cations trapped in solid neon were characterized by absorption spectroscopy. Two electronic transitions were detected for α - and β -HN⁺ in the visible and UV spectral regions, and one for 2-Ime⁺ in the UV. The positions of the band origins and the intensities of the absorptions agree well with the excitation energies and the oscillator strengths of the cations calculated with the CC2 method. The S₂ ← S₀ transition of α -HN⁺ in the

UV is characterized by a strong, broad absorption with weakly discernible vibrational structure suggesting a short S_2 lifetime. Fluorescence was observed upon excitation of α -HN⁺ to its S_1 or S_2 .

Reversible α -HN⁺ \leftrightarrow β -HN⁺ photoisomerization was also observed in these neon matrixes. Excitation to the S_2 state of α -HN⁺ induces a proton transfer in the $\alpha \rightarrow \beta$ direction, whereas β -HN⁺ from its S_1 state decays to S_0 of α -HN⁺ through an out-of-plane conical intersection. The relaxation of β -HN⁺ to α -HN⁺ takes also place on the ground state PES at 6 K. The reversible nature of the α -HN⁺ \leftrightarrow β -HN⁺ phototransformation suggests that protonated PAHs⁺ may be considered as potential systems for designing molecular switches.

■ ASSOCIATED CONTENT

■ Supporting Information

Mass spectra of ions produced in the reaction of naphthalene with protonated methanol; geometry of considered $C_{10}H_9^+$ and $C_{10}H_9$ isomers, and their relative ground-state energy; electronic absorption spectrum of naphthalene radical cation; observed absorption band maxima of electronic transitions of neutral $C_{10}H_9$ radicals; totally symmetric vibrational fundamentals of selected $C_{10}H_9^+$ cations and $C_{10}H_9$ radicals; vertical excitation energies for 1-azulenium and 1-hydro-azulenyl; structures of the S_1/S_0 conical intersections and HOMO and LUMO orbitals of HN⁺. This material is available free of charge via the Internet at <http://pubs.acs.org>.

■ AUTHOR INFORMATION

Corresponding Author

*E-mail: j.p.maier@unibas.ch.

Notes

The authors declare no competing financial interest.

■ ACKNOWLEDGMENTS

This work has been financed by the Swiss National Science Foundation (Project No. 200020-140316/1) and the National Science Centre of Poland (Project No. 2011/01/M/ST2/00561).

■ REFERENCES

- (1) Weilmuenster, P.; Keller, A.; Homann, K. H. *Combust. Flame* **1999**, *116*, 62–83.
- (2) Fialkov, A. B.; Dennebaum, J.; Homann, K. H. *Combust. Flame* **2001**, *125*, 763–777.
- (3) Kiendler, A.; Arnold, F. *Atmos. Environ.* **2002**, *36*, 2979–2984.
- (4) Olah, G. A. *Acc. Chem. Res.* **1971**, *4*, 240–248.
- (5) Olah, G. A.; Mateescu, G. D.; Mo, Y. K. *J. Am. Chem. Soc.* **1973**, *95*, 1865–1874.
- (6) Olah, G. A.; Staral, J. S.; Asencio, G.; Liang, G.; Forsyth, D. A.; Mateescu, G. D. *J. Am. Chem. Soc.* **1978**, *100*, 6299–6308.
- (7) Hudgins, D. M.; Bauschlicher, C. W.; Allamandola, L. J. *Spectrochim. Acta, Part A* **2001**, *57*, 907–930.
- (8) Le Page, V.; Keheyan, Y.; Bierbaum, V. M.; Snow, T. P. *J. Am. Chem. Soc.* **1997**, *119*, 8373–8374.
- (9) Snow, T. P.; Le Page, V.; Keheyan, Y.; Bierbaum, V. M. *Nature* **1998**, *391*, 259–260.
- (10) Pathak, A.; Sarre, P. J. *Mon. Not. R. Astron. Soc.* **2008**, *391*, L10–L14.
- (11) Lorenz, U. J.; Solca, N.; Lemaire, J.; Maitre, P.; Dopfer, O. *Angew. Chem., Int. Ed.* **2007**, *46*, 6714–6716.
- (12) Doublerly, G. E.; Ricks, A. M.; Schleyer, P. V. R.; Duncan, M. A. *J. Phys. Chem. A* **2008**, *112*, 4869–4874.
- (13) Ricks, A. M.; Doublerly, G. E.; Duncan, M. A. *Astrophys. J.* **2009**, *702*, 301–306.
- (14) Jones, W.; Boissel, P.; Chiavarino, B.; Crestoni, M. E.; Fornarini, S.; Lemaire, J.; Maitre, P. *Angew. Chem., Int. Ed.* **2003**, *42*, 2057–2059.
- (15) Knorke, H.; Langer, J.; Oomens, J.; Dopfer, O. *Astrophys. J. Lett.* **2009**, *706*, L66–L70.
- (16) Stuart, A. A. V.; Mackor, E. L. *J. Chem. Phys.* **1957**, *27*, 826–827.
- (17) Reid, C. J. *Am. Chem. Soc.* **1954**, *76*, 3264–3268.
- (18) Dallinga, G.; Mackor, E. L.; Stuart, A. A. V. *Mol. Phys.* **1958**, *1*, 123–140.
- (19) Perkampus, H.; Baumgarten, E. *Angew. Chem., Int. Ed.* **1964**, *3*, 776–783.
- (20) Garkusha, I.; Fulara, J.; Nagy, A.; Maier, J. P. *J. Am. Chem. Soc.* **2010**, *132*, 14979–14985.
- (21) Garkusha, I.; Fulara, J.; Nagy, A.; Maier, J. P. *Astrophys. J.* **2011**, *728*, 131/1–7.
- (22) Garkusha, I.; Fulara, J.; Sarre, P. J.; Maier, J. P. *J. Phys. Chem. A* **2011**, *115*, 10972–10978.
- (23) Alata, I.; Dedonder, C.; Broquier, M.; Marceca, E.; Juvet, C. *J. Am. Chem. Soc.* **2010**, *132*, 17483–17489.
- (24) Alata, I.; Omidyan, R.; Broquier, M.; Dedonder, C.; Dopfer, O.; Juvet, C. *Phys. Chem. Chem. Phys.* **2010**, *12*, 14456–14458.
- (25) Ward, M. D. *J. Chem. Educ.* **2001**, *78*, 321–328.
- (26) Raymo, F. M.; Giordani, S. *Proc. Natl. Acad. Sci.* **2002**, *99*, 4941–4944.
- (27) Auwarter, W.; Seufert, K.; Bischoff, F.; Eciya, D.; Vijayaraghavan, S.; Joshi, S.; Klappenberger, F.; Samudrala, N.; Barth, J. V. *Nanotechnol.* **2012**, *7*, 41–46.
- (28) Liljeroth, P. *Nat. Nanotechnol.* **2012**, *7*, 5–6.
- (29) Hunter, E. P. L.; Lias, S. G. *J. Phys. Chem. Ref. Data* **1998**, *27*, 413–656.
- (30) Fulara, J.; Nagy, A.; Garkusha, I.; Maier, J. P. *J. Chem. Phys.* **2010**, *133*, 024304/1–9.
- (31) Nagy, A.; Fulara, J.; Maier, J. P. *J. Am. Chem. Soc.* **2011**, *133*, 19796–19806.
- (32) Becke, A. D. *J. Chem. Phys.* **1993**, *98*, 5648–5652.
- (33) Dunning, J. T. H. *J. Chem. Phys.* **1989**, *90*, 1007–1023.
- (34) Möller, C.; Plesset, M. S. *Phys. Rev.* **1934**, *46*, 618–622.
- (35) Christiansen, O.; Koch, H.; Jørgensen, P. *Chem. Phys. Lett.* **1995**, *243*, 409–418.
- (36) Hättig, C.; Weigend, F. *J. Chem. Phys.* **2000**, *113*, S154–S161.
- (37) Köhn, A.; Hättig, C. *J. Chem. Phys.* **2003**, *119*, S021–S036.
- (38) Roos, B. O. *Adv. Chem. Phys.* **1987**, *69*, 399–445.
- (39) Ahlrichs, R.; Bär, M.; Häser, M.; Horn, H.; Kölmel, C. *Chem. Phys. Lett.* **1989**, *162*, 165–169.
- (40) Weigend, F.; Häser, M. *Theor. Chem. Acc.* **1997**, *97*, 331–340.
- (41) Frisch, M. J. *Chem. Listy* **2006**, *100*, A9–A9.
- (42) Chong, T.; Shibata, Y.; Itoh, N. *Phys. Status Solidi* **1975**, *27*, 599–604.
- (43) Nakayama, T.; Sheng, S. J. *Mol. Cryst. Liq. Cryst.* **1981**, *69*, 199–206.
- (44) Sebree, J. A.; Kislov, V. V.; Mebel, A. M.; Zwier, T. S. *J. Phys. Chem. A* **2010**, *114*, 6255–6262.
- (45) Rode, M. F.; Sobolewski, A. L.; Dedonder, C.; Juvet, C.; Dopfer, O. *J. Phys. Chem. A* **2009**, *113*, 5865–5873.
- (46) Lias, S. G.; Ausloos, P. J. *Chem. Phys.* **1985**, *82*, 3613–3624.
- (47) Bouchoux, G.; Nguyen, M. T.; Salpin, J. Y. *J. Phys. Chem. A* **2000**, *104*, 5778–5786.
- (48) Herman, J. A.; Herman, K.; McMahon, T. B. *Can. J. Chem.* **1991**, *69*, 2038–2043.
- (49) Pettersson, M.; Maçôas, E. M. S.; Khriachtchev, L.; Lundell, J.; Fausto, R.; Räsänen, M. *J. Chem. Phys.* **2002**, *117*, 9095–9098.
- (50) Marushkevich, K.; Khriachtchev, L.; Räsänen, M. *J. Chem. Phys.* **2007**, *126*, 241102/1–4.
- (51) Knight, L. B.; Steadman, J.; Feller, D.; Davidson, E. R. *J. Am. Chem. Soc.* **1984**, *106*, 3700–3701.
- (52) Paddon-Row, M. N.; Fox, D. J.; Pople, J. A.; Houk, K. N.; Pratt, D. W. *J. Am. Chem. Soc.* **1985**, *107*, 7696–7700.